J. Fluid Mech. (1984), *vol.* 142, *pp.* 57–77
Printed in Great Britain

Contaminant dispersion in some time-dependent laminar flows

By C. JIMENEZ AND P. J. SULLIVAN
Department of Applied Mathematics, University of Western Ontario, London, Canada

(Received 2 May 1983 and in revised form 28 November 1983)

Time-dependent flows occur naturally as in pulsatile blood flow and in tidal estuaries and comprise many of the man-made flows of practical importance. A knowledge of the rate of mixing of a contaminant substance in such time-dependent flows is of paramount interest in, for example, the injection of a chemical substance in blood flow, the discharge of outfalls in estuaries, and the mutual contamination length of two feed fluids when switching from one feed line to another as part of a manufacturing process. This paper presents a study of contaminant spread in two specific and well-defined flows and provides a basis for the interpretation of contaminant mixing in the more complex flow situations that normally prevail.

An extension of the probabilistic formulation of the streamwise dispersion of contaminant molecules given in Dewey & Sullivan (1982) is used to study time-dependent laminar flows between parallel plates and in tubes wherein the flows are homogeneous in the streamwise direction. The two flows considered in detail are oscillating flows and impulsively started flows. In impulsively started flows it is shown that, although the basic dispersive mechanism acts in much the same way as described by Taylor (1953), the start-up effects on the dispersion can be quite prolonged and very significantly reduce the streamwise spread of contaminant over that which is observed in the fully developed flow. In oscillatory flows, unlike the situation presented by Taylor (1953) in which a diminished value of molecular diffusivity κ increases the contaminant cloud axial growth rate in a tube of radius a, it is found that optimal streamwise contaminant spread results from a value of κ that depends upon kinematic viscosity ν and frequency ω. The streamwise cloud-variance growth rate is explored over the full range of the two parameters $\gamma^2 = \omega a^2/\kappa$ and $\lambda^2 = \omega a^2/2\nu$ for all time, and it is shown that a global maximum results when $\gamma \approx 2\pi$ and $\lambda \approx 2$.

1. Introduction

Taylor (1953) showed that the dominant mechanism whereby a scalar contaminant cloud is spread out in the steady flow within a tube is dispersion – the interaction between the molecular diffusivity in the radial direction and the gradient of the axial component of the mean-flow velocity. Taylor showed that following a reasonably long period of time, $t\kappa/a^2 \gg 1$, the dispersive contribution to the growth rate of the streamwise cloud variance σ^2 is given by

$$\frac{\mathrm{d}}{\mathrm{d}t}\sigma^2 \sim \frac{U^2 a^2}{\kappa}, \tag{1}$$

where U is the average flow velocity. It is apparent from (1) that $\mathrm{d}\sigma^2/\mathrm{d}t \to 0$ as $\kappa \to \infty$, corresponding to each constituent cloud molecule moving at all times with velocity U, and $\mathrm{d}\sigma^2/\mathrm{d}t \to \infty$ as $\kappa \to 0$, corresponding to each constituent cloud molecule

retaining its initial velocity for all time. By contrast, in an oscillating flow the change in cloud variance following one cycle when $\kappa \to 0$ is zero, since the constituent molecules all return to their initial release positions, and will also be zero when $k \to \infty$, for the same reason as for a steady flow. One then expects, for this rather different dispersion phenomenon, some optimal dispersion effect for a value of κ intermediate to these extreme values.

The velocity profile in the steady laminar flow within a tube is always parabolic. The velocity profile of an oscillatory flow can be drastically altered by a change in the frequency ω and the kinematic viscosity ν. There the dispersion is governed by the two parameters λ and γ, where $\lambda^2 = \omega a^2/2\nu$ and $\gamma^2 = \omega a^2/\kappa$, which represent the number of periods required for vorticity and scalar contaminant respectively to diffuse over the cross-section.

A considerable amount of work has been done for oscillating flows without phase lag in the flow velocity across the conduit and especially at large times. For example Smith (1982*a*) has shown the sensitivity to time of release of contaminant during a cycle and also the importance of the location of a discharge source (Smith 1982*b*) on the flow cross-section. Smith (1983) has also given the time evolution of the lower-order statistical moments of a contaminant cloud and shown these to have a reasonable agreement with Allen's (1982) random-walk result for a turbulent, oscillating, open-channel flow model. The principal results of this paper are due directly to the phase-lag of the velocity at different positions on the flow cross-section of a laminar flow. The use of these results in the time-dependent turbulent-flow problem where the cross-sectional mixing is time-dependent is the subject of a forthcoming paper (see Chatwin & Sullivan 1984). Chatwin (1975) has shown that the simple Gaussian form for the cross-sectionally integrated streamwise contaminant concentration $C(x, t)$ that was found by Taylor (1953) for a steady flow is retrieved after a sufficiently long time in oscillatory flows. However, as in the case of steady flows, the asymptotic behaviour develops too slowly to be of much general use, and in this paper a full description of the variance growth rate is developed for a complete range of λ and γ for all time.

The dispersion of contaminant in two specific time-dependent flows is explored. The oscillatory flows that result from a sinusoidal pressure difference over the ends of a tube (and away from the end regions) and the impulsively started flows, which would result from the sudden opening of a valve in a pipeline, for example, are both flows that are homogeneous in the streamwise direction. For ease of exposition a very detailed investigation is provided for these time-dependent flows between parallel plates, and the corresponding results (which do not change in character) are merely stated for the tube geometry. In all cases considered, the initial contaminant cloud is taken to be a thin uniform sheet of contaminant over the flow cross-section.

2. General formulation

The formulation that follows is an extension of that given in Dewey & Sullivan (1982), and takes into account the time dependence of the Eulerian velocity field. One is concerned here with flows within arbitrarily shaped but uniform conduits that do not change in the streamwise x-direction (see figure 1). The Lagrangian streamwise displacement $X(t; \boldsymbol{y}_0)$ of a fluid molecule at time t that was released at time t_0 at a position on the cross-section located by the (two-dimensional) vector $\boldsymbol{y}_0$ and $x = 0$ (i.e. $X(t_0; \boldsymbol{y}_0) = 0$) is determined from

$$X(t; \boldsymbol{y}_0) = \int_{t_0}^{t} v(\tau; \boldsymbol{y}_0)\, \mathrm{d}\tau, \tag{2}$$

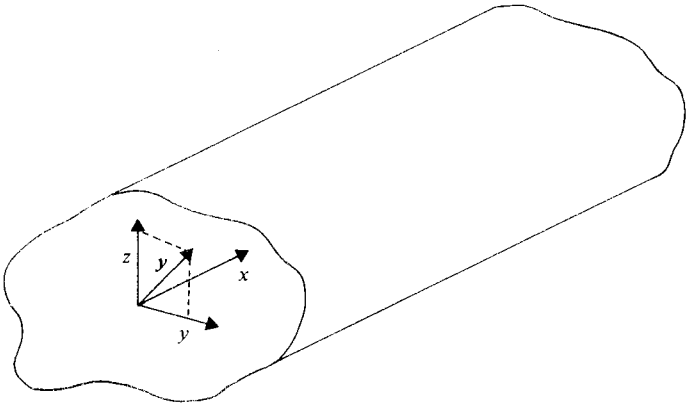

FIGURE 1. A sketch of the basic geometrical configuration considered in §2.

where $v(\tau;\boldsymbol{y}_0)$ is the Lagrangian streamwise component of the molecule's velocity. The second moment of the displacement, following Taylor (1921), when one event of the ensemble is the release of a uniform sheet of molecules over the plane $x = 0$, is found from

$$\frac{1}{2}\frac{\mathrm{d}\overline{X^2(t;t_0)}}{\mathrm{d}t} = \frac{1}{A}\int_A \mathrm{d}A(\boldsymbol{y}_0)\int_{t_0}^{t} \overline{v(t;\boldsymbol{y}_0)\,v(\tau;\boldsymbol{y}_0)}\,\mathrm{d}\tau, \tag{3}$$

where A is the cross-sectional area and an overbar is used to denote an ensemble average. The Lagrangian molecule velocity $v(t;\boldsymbol{y}_0)$ can be expressed in terms of the Eulerian flow velocity $u(\boldsymbol{y},t)$ as

$$v(t;\boldsymbol{y}_0) = u(\boldsymbol{Y}(t;\boldsymbol{y}_0)) + w', \quad \overline{w'} = 0, \tag{4}$$

where $\boldsymbol{Y}(t;\boldsymbol{y}_0)$ is the Lagrangian cross-stream displacement vector and w' is the random microscopic streamwise velocity fluctuation due to thermal molecular activity. The use of (4) in (3) results in

$$\frac{1}{2}\frac{\mathrm{d}\overline{X^2(t;t_0)}}{\mathrm{d}t} = \frac{1}{A}\int \mathrm{d}A(\boldsymbol{y}_0)\int_{t_0}^{t} \overline{u(\boldsymbol{Y}(t;\boldsymbol{y}_0))\,u(\boldsymbol{Y}(\tau;\boldsymbol{y}_0))}\,\mathrm{d}\tau \tag{5}$$

when the small additive constant κ is neglected; which, using the appropriate ensemble-average values of (2), provides the growth rate of the cloud variance

$$\frac{1}{2}\frac{d\sigma^2(t;t_0)}{\mathrm{d}t} = \frac{1}{A}\int_A \mathrm{d}A(\boldsymbol{y}_0)\int_{t_0}^{t} \overline{u(\boldsymbol{Y}(t;\boldsymbol{y}_0))\,u(\boldsymbol{Y}(\tau;\boldsymbol{y}_0))}\,\mathrm{d}\tau - U(t)\int_{t_0}^{t} U(\tau)\,\mathrm{d}\tau, \tag{6}$$

where

$$U(t) = \frac{1}{A}\int_A u(\boldsymbol{y},t)\,\mathrm{d}A(\boldsymbol{y}) \tag{7}$$

is the average flow velocity.

With an event in the ensemble – the release of a uniform sheet of contaminant molecules over the uniform conduit cross-section – the distribution of contaminant over the cross-section remains uniform for all time. For every path that takes a molecule from $\boldsymbol{y}_0$ at t_0 to $\boldsymbol{y}$ at t there will be one identical path in the ensemble that

takes a molecule from $\boldsymbol{y}$ at t_0 to $\boldsymbol{y}_0$ at t. The correlation integral in (6) can be rewritten in terms of equivalent paths of $\boldsymbol{Y}(t;\boldsymbol{y}_0)$ as

$$\int_{t_0}^{t} \overline{u(\boldsymbol{Y}(t_0;\boldsymbol{y}_0),t)\,u(\boldsymbol{Y}(t+t_0-\tau;\boldsymbol{y}_0),\tau)}\,\mathrm{d}\tau. \tag{8}$$

In (8) $u(\boldsymbol{Y}(t_0;\boldsymbol{y}_0),t)$ is deterministic with respect to the ensemble average, and the mean-velocity history $\overline{u(\boldsymbol{Y}(t+t_0-\tau;\boldsymbol{y}_0),\tau)}$ is found from

$$\overline{u(\boldsymbol{Y}(t+t_0-\tau;\boldsymbol{y}_0),\tau)} = \int_A u(\boldsymbol{y},\tau)\,p(\boldsymbol{y},t+t_0-\tau;\boldsymbol{y}_0)\,\mathrm{d}A(\boldsymbol{y}), \tag{9}$$

where p satisfies

$$\frac{\partial p}{\partial t} = \nabla^2 p, \tag{10}$$

$$\frac{\partial p}{\partial n} = 0 \quad \text{on } \Gamma, \quad \lim_{t\to\infty} p = \frac{1}{A}, \tag{11}$$

$$p(\boldsymbol{y},t_0) = \delta(y-y_0)\,\delta(z-z_0) \tag{12}$$

and where ∇^2 is the two-dimensional Laplacian operator, n is the normal to the conduit boundary Γ, and y_0 and z_0 are the components of the position vector $\boldsymbol{y}_0$. Thus the growth rate of the streamwise variance is determined from the probability $p(\boldsymbol{y},t;\boldsymbol{y}_0)\,\mathrm{d}A(\boldsymbol{y})$ that a fluid molecule released at $\boldsymbol{y}_0$ at time t_0 will be within an area element $\mathrm{d}A$ centred on $\boldsymbol{y}$ at time t and from the Eulerian velocity profile $u(\boldsymbol{y},t)$ as

$$\frac{1}{2}\frac{\partial\sigma^2}{\partial t}(t;t_0) = \frac{1}{A}\int_A \mathrm{d}A(\boldsymbol{y}_0)\int_A \mathrm{d}A(\boldsymbol{y})\int_0^{t-t_0} u(\boldsymbol{y}_0,t)\,u(\boldsymbol{y},t-\tau)\,p(\boldsymbol{y},\tau+t_0;\boldsymbol{y}_0)\,\mathrm{d}\tau - U(t)\int_{t_0}^{t} U(\tau)\,\mathrm{d}\tau. \tag{13}$$

The longitudinal dispersivity $\frac{1}{2}\,\mathrm{d}\sigma^2/\mathrm{d}t$ could also have been calculated using the method put forward by Aris (1956) in a somewhat less-straightforward and less-physical manner, and the two methods are shown to give the same result in Appendix A. Quite apart from the current subject of interest, the same basic approach as presented here can be used to formulate the time-dependent turbulent flow problem using approximations like those given in Dewey & Sullivan (1979). Two critical conditions that were necessary in the foregoing analysis were that the initial contaminant cloud be uniformly distributed over the flow cross-section and that the flow be homogeneous in the streamwise direction. In what follows, two specific flows that can be made to meet these conditions, oscillatory flows and impulsively started flows, are analysed in detail.

3. Oscillatory flows

The steady-state streamwise velocity profile $u'(y',t')$ of the incompressible, oscillatory flow between two parallel plates located at $y' = \pm a'$ that satisfies

$$\frac{\partial u'}{\partial t} = G\cos(\omega t') + \nu\frac{\partial^2 u'}{\partial y'^2} \tag{14}$$

subject to

$$u'(\pm a,t') = 0 \tag{15}$$

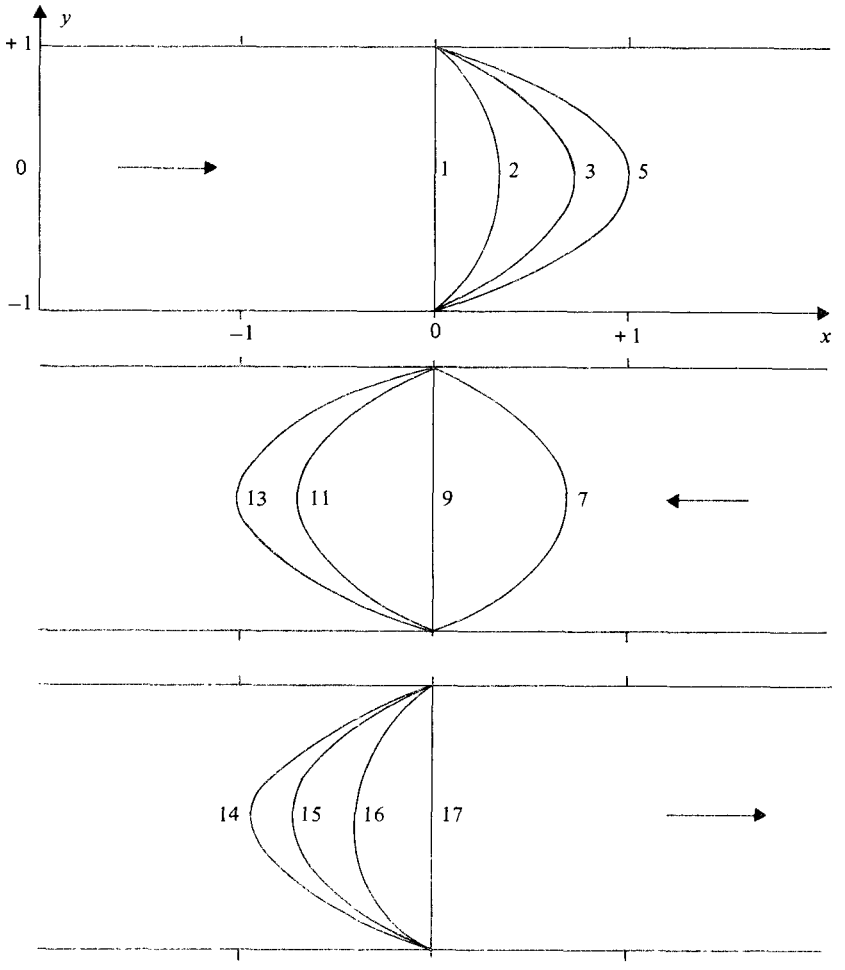

(*a*)
Case λ = 0.1

FIGURE 2(*a*). For caption see p. 63.

can be readily confirmed to be

$$u(y,t) = \frac{1-c_0(\lambda y)\,c_0(\lambda)+s_0(\lambda y)\,s_0(\lambda)}{c_0^2(\lambda)+s_0^2(\lambda)}\sin t+\frac{c_0(\lambda y)\,s_0(\lambda)-s_0(\lambda y)\,c_0(\lambda)}{c_0^2(\lambda)+s_0^2(\lambda)}\cos t$$

$$= g(\lambda,y)\sin t+h(\lambda,y)\cos t$$

$$= A(\lambda,y)\cos\left(t-\rho(\lambda,y)\right), \tag{16}$$

where
$$A^2 = g^2+h^2, \quad \rho = \tan^{-1}\frac{g}{h}. \tag{17}$$

In (16)
$$c_0(y) = \cosh y\cos y, \tag{18}$$

$$s_0(y) = \sinh y\sin y, \tag{19}$$

and the variables have been non-dimensionalized as $u = \omega u'/G, x = \omega^2 x'/G$, $y = y'/a, t = \omega t'$ and also $\lambda^2 = \omega a^2/2\nu$.

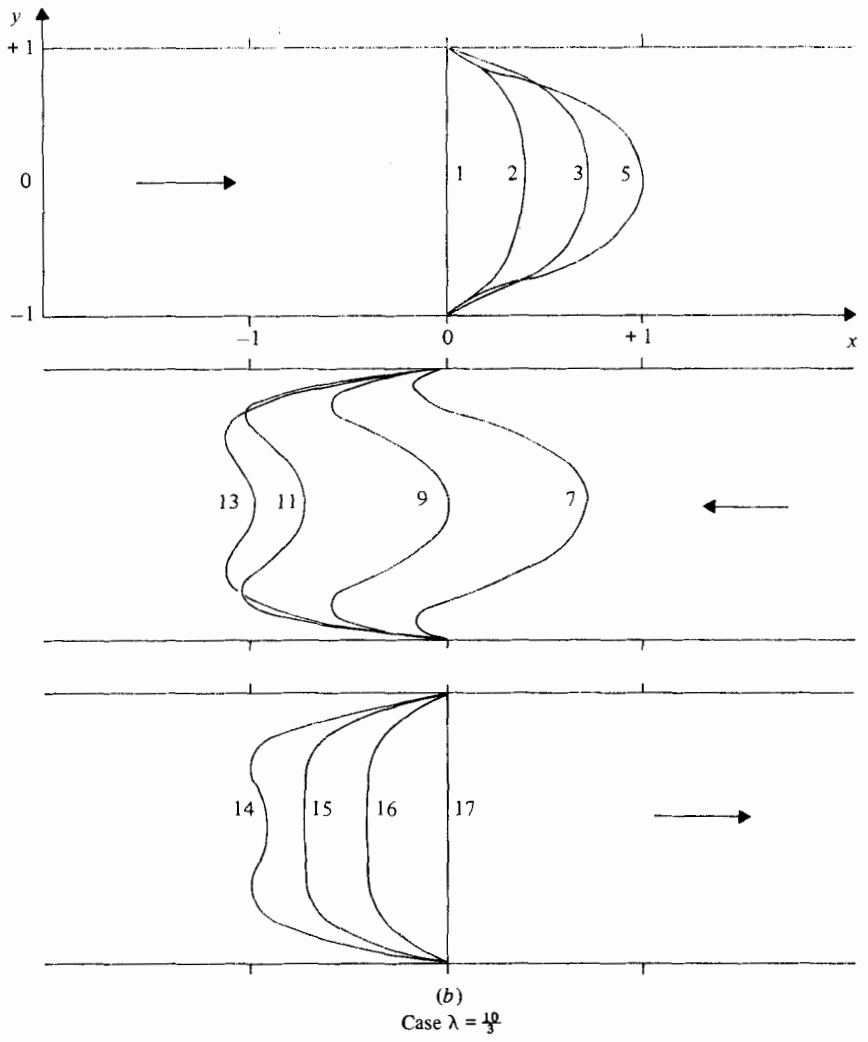

FIGURE 2(*b*). For caption see facing page.

It is of interest to consider the displacement of a line of contaminant placed across the flow (i.e. dispersion with $\kappa = 0$). The time of release t_0 is chosen so that contaminant at $y = 0$ oscillates around $x = 0$ with zero phase angle. If $\hat{X}(y, t-t_0)$ is the displacement of contaminant located at y then

$$\frac{\hat{X}(y, t-t_0)}{A(0)} = \frac{A(y)}{A(0)} \sin\,(t-\rho(y)) \tag{20}$$

is the displacement, normalized with the $y = 0$ amplitude, and

$$t_0 = \tan^{-1} \frac{c_0^2(\lambda) + s_0(\lambda)^2 - c_0(\lambda)}{s_0(\lambda)}. \tag{21}$$

Figures 2(*a*, *b*, *c*) show respectively the displacement profiles of (20) corresponding to

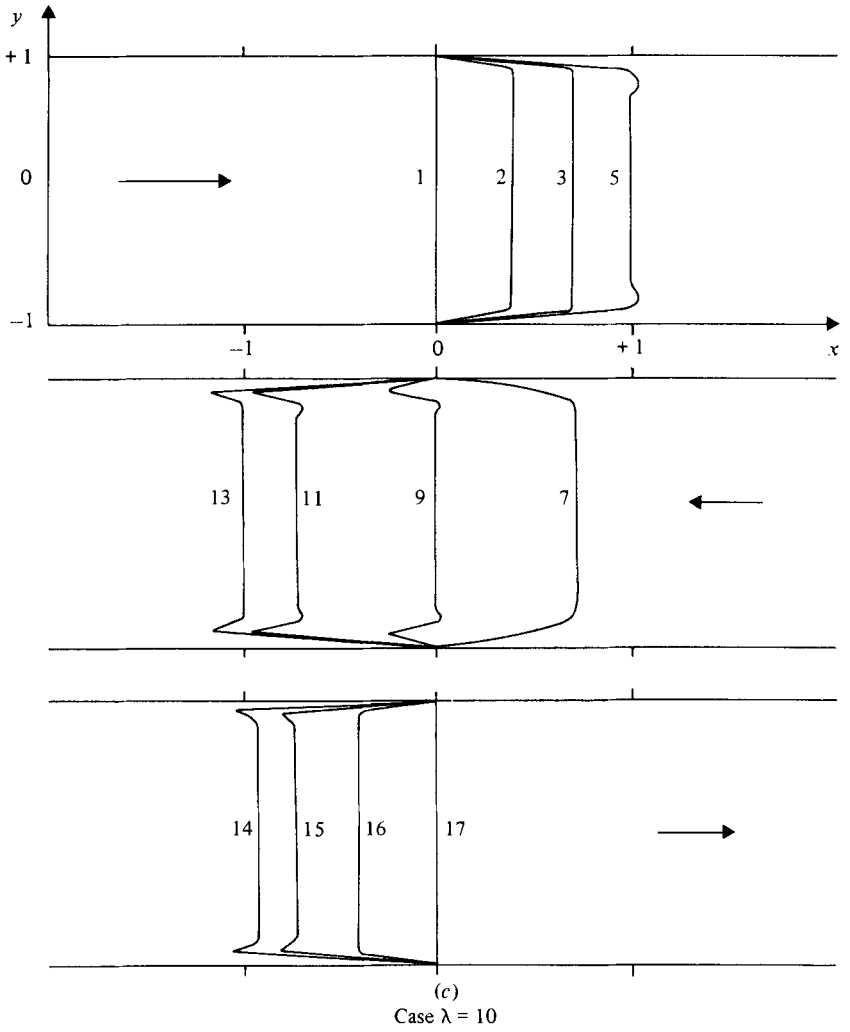

FIGURE 2. The displacement of a line of contaminant ($\kappa = 0$) that is embedded in the flow such that the mid-plate displacement has zero phase and normalized with the mid-plate displacement amplitude. The numbers on the figures correspond to values of K where $t = \frac{1}{16}(k-1)\pi$.

the $\lambda \ll 1$ 'sloshing-mode', the $\lambda = \frac{10}{3}$ value which is approximately where the largest overall amplitude A occurs, and the $\lambda \gg 1$ boundary-layer behaviour of (16). It is worth noting the large variety of displacement shapes that occur in general, and specifically the significant degree of curvature in $\bar{X}$ present in figure 2(*b*), which results from the phase difference and which certainly will have a significant effect on the dispersion process.

The dispersion of a contaminant sheet can now, with (13), be written in terms of the Eulerian velocity profile (16) and the probability density function p, which is known from Dewey & Sullivan (1979) for this geometry and non-dimensionalization to be

$$p(y,t;y_0) = \sum_{n=1}^{\infty} \mathrm{e}^{-(n\pi/2\gamma)^2} \cos\tfrac{1}{2}n\pi\,(y+1)\cos\tfrac{1}{2}n\pi\,(y_0+1)+\tfrac{1}{2}, \quad p = p'a. \tag{22}$$

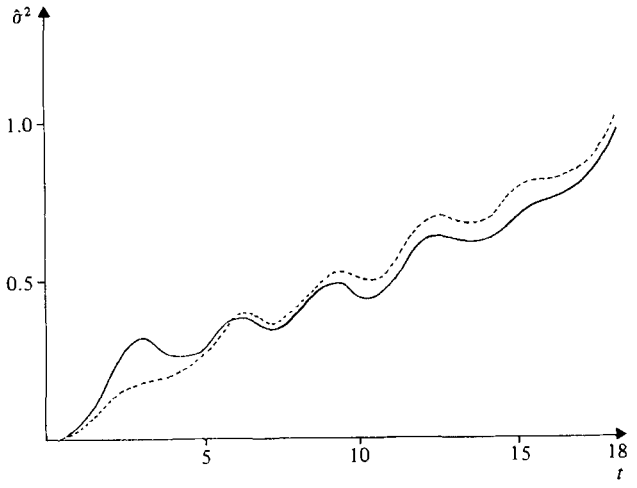

FIGURE 3. A comparison between the simulated (– – –) and calculated (——) values of the non-dimensional variance when $\lambda = 2$ and $\gamma = 3\sqrt{2}$ (see (23)) for the oscillating flow between parallel plates.

Specializing, for ease of exposition, to the case where $t_0 = 0$ in (13), and using (22) and (16), the growth rate of the non-dimensional streamwise variance $\hat{\sigma}^2$ is found to be (after some manipulation that is recorded in more detail in Jimenez 1982)

$$\frac{1}{2}\frac{\mathrm{d}\hat{\sigma}(t)^2}{\mathrm{d}t} = \sum_{n=1}^{\infty} \left\{ \frac{R_n(\lambda)\sin t + S_n(\lambda)\cos t}{1+(n\pi/\gamma)^4} \right\} \left\{ \left(\left(\frac{n\pi}{\gamma}\right)^2 R_n(\lambda) + S_n(\lambda) \right) \sin t \right.$$
$$\left. + \left(\left(\frac{n\pi}{\gamma}\right)^2 S_n(\lambda) - R_n(\lambda) \right) \cos t + \left(R_n(\lambda) - \left(\frac{n\pi}{\gamma}\right)^2 S_n(\lambda) \right) \mathrm{e}^{-(n\pi/\gamma)^2 t} \right\}, \quad (23)$$

where

$$R_n(\lambda) = \left\{ \begin{array}{ll} \dfrac{-B_n \sin 2\lambda - A_n \sinh 2\lambda}{2(c_0^2(\lambda) + s_0^2(\lambda))} & (n \text{ even}), \\ 0 & (n \text{ odd}), \end{array} \right\} \quad (24)$$

$$S_n(\lambda) = \left\{ \begin{array}{ll} \dfrac{B_n \sinh 2\lambda - A_n \sin 2\lambda}{2(c_0^2(\lambda) + s_0^2(\lambda))} & (n \text{ even}), \\ 0 & (n \text{ odd}), \end{array} \right\} \quad (25)$$

$$A_n = \frac{\lambda}{\lambda^2 + (\frac{1}{2}n\pi + \lambda)^2} + \frac{\lambda}{\lambda^2 + (\frac{1}{2}n\pi - \lambda)^2}, \quad (26)$$

$$B_n = \frac{\lambda + \frac{1}{2}n\pi}{\lambda^2 + (\frac{1}{2}n\pi + \lambda)^2} + \frac{\lambda - \frac{1}{2}n\pi}{\lambda^2 + (\frac{1}{2}n\pi - \lambda)^2}. \quad (27)$$

It is clear from (23) that the transient effects decay away at $t\gamma^{-2} = t'\kappa a^{-2} = O(1)$ and in a way that is consistent with Chatwin (1975). That is in the time taken for contaminant molecules to sample the depth a. Figure 3 shows the variance as calculated from (23) when $\lambda = 2$ and $\gamma = 3\sqrt{2}$, which are approximately the parameters in use in figure 2(*b*). A considerably simplified expression for (23) results

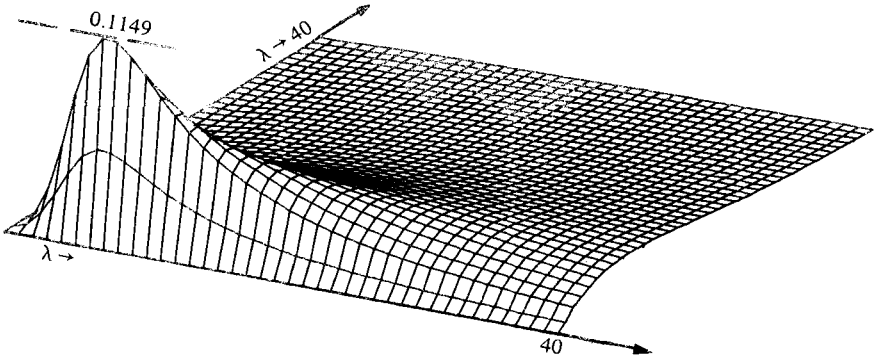

FIGURE 4. The surface of large-time non-dimensional variance increment $\Delta\sigma^2(\lambda, \gamma)$ in one cycle for the oscillating flow between parallel plates as calculated from (28).

when one considers $t \gg \gamma^2$ and the change in non-dimensional variance that takes place in one period

$$\Delta\sigma^2(\gamma, \lambda) = \int_T^{T+2\pi} \frac{1}{2\pi} \frac{\mathrm{d}\hat{\sigma}^2(\tau)}{\mathrm{d}t} \mathrm{d}\tau$$

$$= \sum_{n=1}^{\infty} \left(\frac{n\pi}{\gamma}\right)^2 \frac{R_n^2(\lambda) + S_n^2(\lambda)}{1 + (n\pi/\gamma)^4}. \tag{28}$$

The surface $\Delta\sigma^2(\lambda, \gamma)$ is shown on figure 4. The most prominent feature on the surface of figure 4 is a global maximum value of $\Delta\sigma^2 \approx 0.1149$ when $\lambda \approx 2$ and $\gamma \approx 2\pi$.

To explain the location of the global maximum of $\Delta\sigma^2$ one needs to construct the best circumstances for increasing $\Delta\sigma^2$ in one cycle. Consider the displacement of a line of contaminant as shown on figures 2(*a–c*). One expects the largest increase in variance when κ is sufficiently large to diffuse contaminant material uniformly across the conduit in one half-cycle (or actually just short of this, to give weight to having the largest values of contaminant concentration as far removed from $x = 0$ as possible) that is $\gamma = O(1)$. The lower the value of κ that will provide this type of distribution, the higher will be the values of concentration at large x at the end of a cycle, and hence the largest values of $\Delta\sigma^2$. One notices, because of the large curvature of the contaminant line on the return cycle in figure 2(*b*), that a smaller value of κ (i.e. larger γ) will effect the same degree of cross-stream mixing on the return cycle as those profiles in figure 2(*a*), and thus leave a residue of larger contaminant concentration values at large x. Another way of stating this is that for the self-similar profiles shown in figure 2(*a*) contaminant that diffuses away from the line of contaminant in the first quarter-cycle has a tendency to diffuse back toward the line on the return stroke. In terms of a typical molecule's velocity for these self-similar profiles, a molecule that wanders into a region of the flow that has a velocity in defect of the mean-flow velocity on the outgoing stroke will likely be in a region of the flow where the velocity is in excess of the mean-flow velocity on the return stroke (see (13)) and thereby minimize the contribution to $\Delta\sigma^2$. The phase differences that are shown in figure 2(*b*) make it possible for a typical molecule to sample relatively large velocity variations with a small value of κ. One also notices that the global maximum of $\Delta\sigma^2$ occurs approximately at a value of $\lambda = \frac{10}{3}$, which provides the overall maximum value of velocity as well as the large phase changes that are shown on figure 2(*b*).

In the sequence of figures 5 (a, b) and 7 (a, b) the contaminant molecule distribution on the flow cross-section that was found using a numerical simulation are shown for the two interesting cases of the optimal conditions for dispersion and of the boundary-layer-type behaviour. This simulation is the result of a computer program that follows individual contaminant molecules as these do a random walk over the flow cross-section and is described in Appendix B.

In figure 5 (a), corresponding to the optimal $\Delta\sigma^2$, it is clear in the outgoing stroke ($t \leqslant 2.25$) that there is little cross-sectional mixing and that very high values of contaminant concentration are retained near $y = 0$. On the return stroke, and almost immediately ($2.25 \leqslant t \leqslant 3.6$), contaminant is rapidly spread over the cross-section leaving a considerable residue at the end of the half-cycle over a considerable distance in x. The stroke is completed with the central ($y \sim 0$) region of the flow following the ($y \sim 1$) wall region in the negative direction and ultimately returning to the start position ($t \sim 5$), where contaminant molecules are in a reasonably uniform distribution over the ($x \sim 0$) cross-section. Figure 6 (a, b) shows the x-distribution of molecules (that is, the sum of the values shown in figure 5 over the y-direction). The effect of phase change and low κ is apparent here by the large peak value that exists at the end of the first quarter stroke. As the reverse flow occurs, the high levels of contaminant near the central core region and proceeding in a negative direction is diffused into the wall regions, which are out of phase with the central core and going in the opposite direction so that the high peak values can be traced throughout the entire cycle.

It is also interesting to observe the boundary-layer effect as shown in figures 7 (a, b). There, a central core ($y \sim 0$) of high contaminant-concentration values persist throughout the entire half-cycle, and the dispersion is taking place, in the main, by virtue of the small fraction of contaminant located in the wall layer. The integrated values shown on figure 8 show a high peak value that represents the core contaminant, and this remains well defined throughout the entire cycle.

Flows with λ and γ of order unity can readily be achieved in gases. For example, with air ($\nu = 0.144$ cm^2/s, $\kappa = 0.219$ cm^2/s a separation of a few centimetres leads to $\omega \sim 1$ rad/s. In liquids this is somewhat less common because of the high (10^3) value of the Schmidt number. However, for example, with water ($\nu = 0.01$ cm^2/s, $\kappa = 1.3 \times 10^{-5}$ cm^2/s for a saline solution) values of a few centimetres and a 2 h cycle for ω provide values of $\gamma \approx 9$ and $\lambda \approx 0.2$.

The oscillatory flow within a tube that satisfies

$$\frac{\partial u'}{\partial t'} = G \cos \omega t' + \frac{\nu}{r'} \frac{\partial}{\partial r'} \left(r' \frac{\partial u'}{\partial r'} \right) \tag{29}$$

and

$$u'(a, t) = 0 \quad (0 \leqslant r' \leqslant a) \tag{30}$$

has been discussed at length in Schlicting (1960).

The solution to (29) can be written as a Fourier–Bessel expansion

$$u = 2 \sum_{n=1}^{\infty} \frac{\lambda^2 \sin t + \eta_n \cos t}{\eta_n (\lambda^4 + \eta_n^4)} \frac{J_0(r\eta_n)}{J_1(\eta_n)}, \tag{31}$$

where η_n is the nth root of $J_0(\eta_n) = 0$, and $r = r'/a$.

The probability density function $p(r, t; r_0)$ corresponding to (10)–(12) is found from the solution of

$$\frac{\partial p}{\partial t} = \frac{\kappa}{r} \frac{\partial}{\partial r} \left(r \frac{\partial p}{\partial r} \right), \tag{32}$$

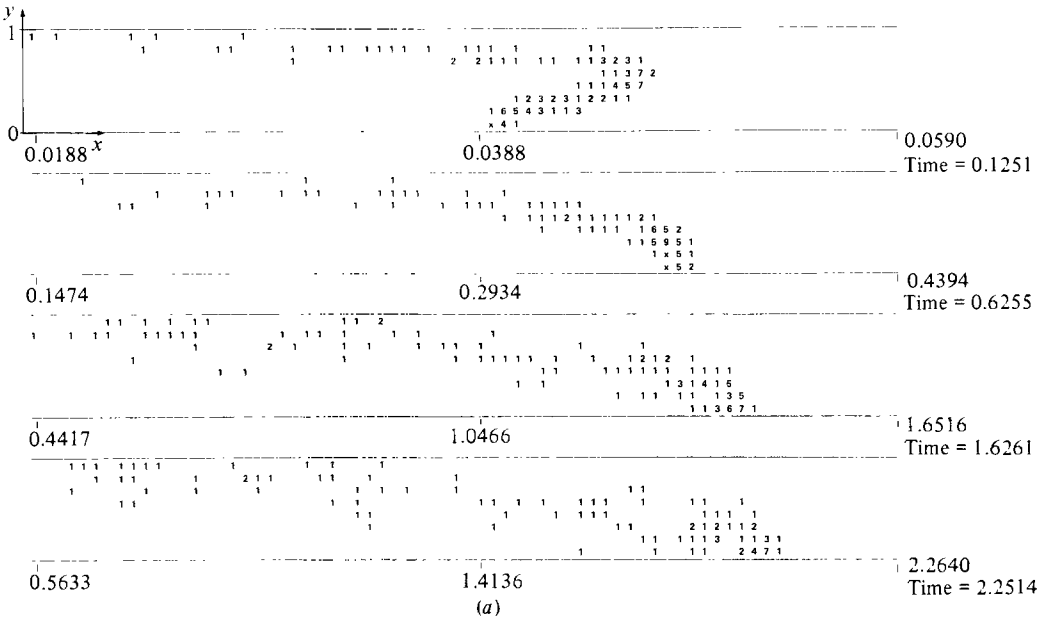

(*a*)

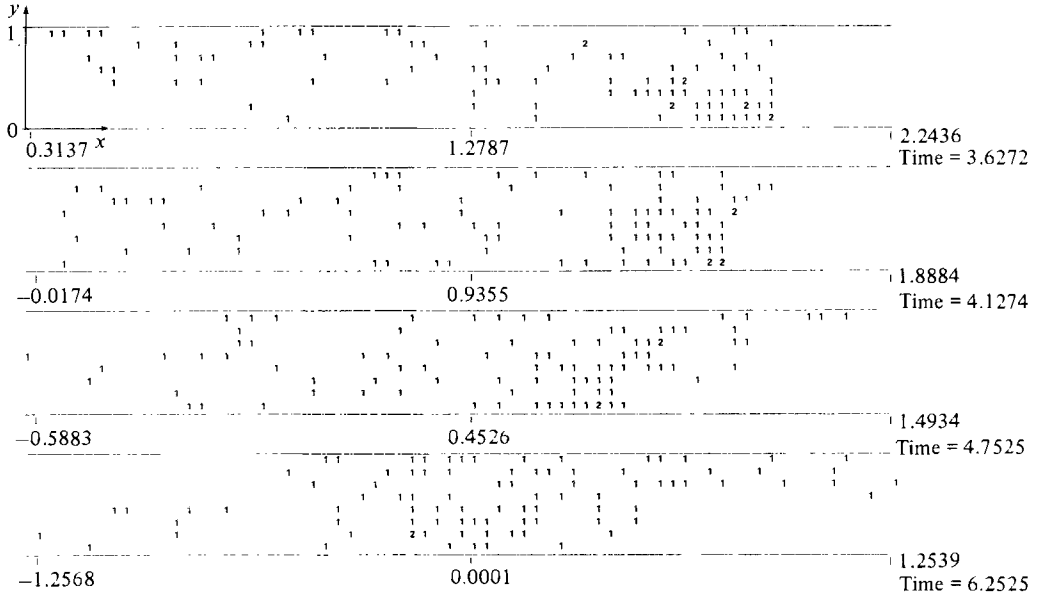

(*b*)

FIGURE 5. A numerical simulation of the evolution of a pulse of contaminant between parallel plates with an oscillating flow for which $\lambda = 2$ and $\gamma = 3\sqrt{2}$. A single integer is used to indicate the number of contaminant molecules within discrete area elements on the interval $\bar{X} \pm 0.96\sigma$. 1 indicates between 4 and 9 molecules, 2 indicates between 10 and 14 molecules, etc. An asterisk shows an offscale value (this is never greater than 81 molecules).

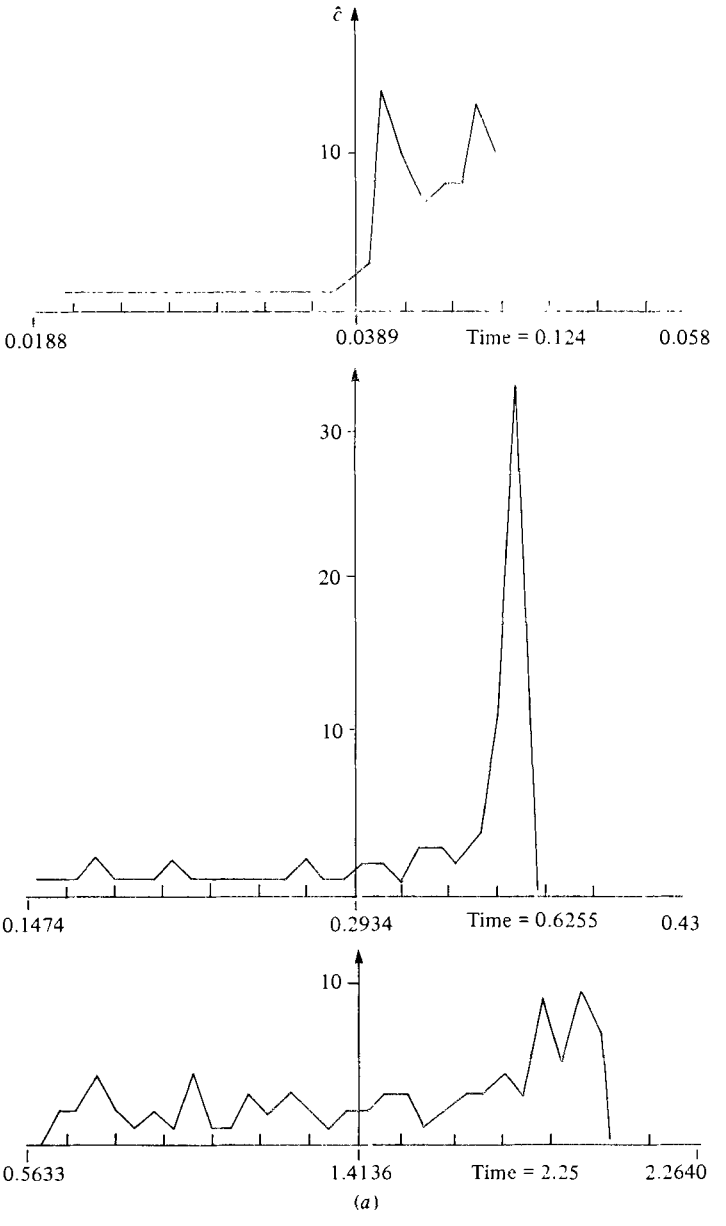

FIGURE 6(*a*). For caption see facing page.

$$\frac{\partial p}{\partial r} = 0 \quad \text{on} \quad r = a, \tag{33}$$

$$p(r, 0, r_0) = \delta(r - r_0)/2\pi \tag{34}$$

to be

$$p(r, t; r_0) = \frac{1}{\pi} \sum_{n=1}^{\infty} J_0(r_0 \xi_n) \, \mathrm{e}^{-(\xi_n/\gamma)^2 t} \frac{J_0(r\xi_n)}{J_1(\xi_n)^2}. \tag{35}$$

The use of (35) and (31) in (13) results in the longitudinal dispersivity

$$\frac{1}{2}\frac{\mathrm{d}\hat{\sigma}^2(t)}{\mathrm{d}t} = \frac{1}{\pi} \sum_{q,p,n=1}^{\infty} \frac{\lambda^2 \sin t + \eta_p \cos t}{(\lambda^4 + \eta_p^4)(\xi_q^2 - \eta_p^2)(\xi_q^2 - \eta_n^2)} \int_0^t \frac{\lambda^2 \sin \tau + \eta_n \cos \tau}{(\lambda^4 + \eta_n^4)} \, \mathrm{e}^{-(\xi_q/\gamma)^2 (t-\tau)} \, \mathrm{d}\tau, \tag{36}$$

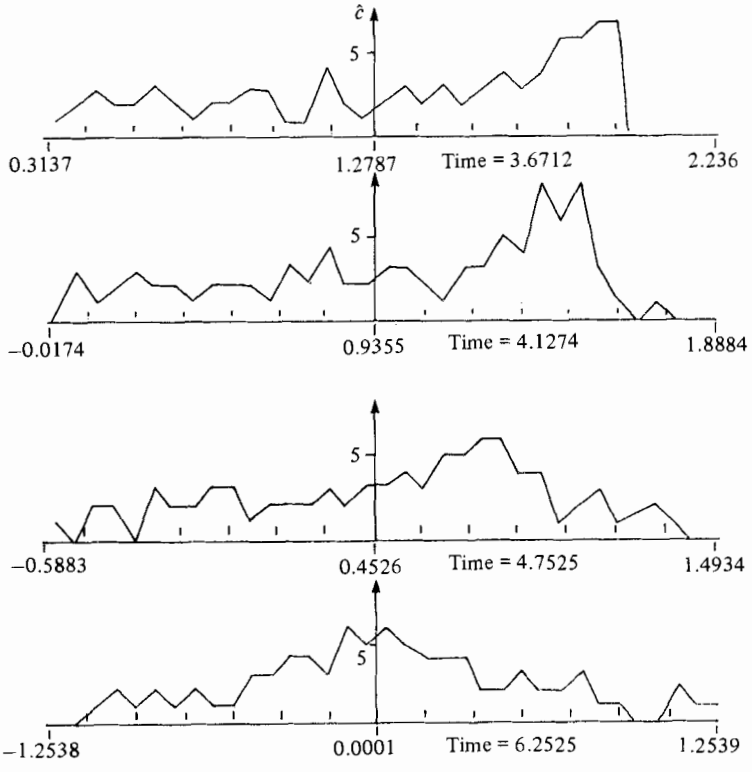

(*b*)

FIGURE 6. A summation over the depth of the simulated location of molecules displayed in figure 5 on the interval $\bar{X} \pm 1.96\sigma$ and expressed as a percentage.

which is observed to degenerate, following a long period of time from release at $t = 0$, to the form

$$\frac{1}{2}\frac{\mathrm{d}\hat{\sigma}^2}{\mathrm{d}t} \sim A_0 + A_1 \sin^2 t + A_2 \cos^2 t, \tag{37}$$

where the constants A_0, A_1 and A_2 depend on λ and γ, as found by Chatwin (1975). One expects (36) to produce, in essence, the same type of surface shown in figure 4 for the parallel-plate geometry.

4. Impulsively started flows

Dispersion in impulsively started flows more closely resembles the dispersion described by Taylor (1953) than in oscillatory flows. One can here assess the contribution that is made to streamwise dispersion by the adjustments of the mean-stream-velocity profile in reaching its steady-state value.

For the parallel-plate geometry outlined in §2 the solution of

$$\frac{\partial u'}{\partial t'} = GS(t') + \nu \frac{\partial^2 u'}{\partial y'^2} \tag{38}$$

with

$$u'(\pm a, t') = 0 \quad (-a \leqslant y' \leqslant a) \tag{39}$$

and

$$-\frac{1}{\rho}\frac{\mathrm{d}p}{\mathrm{d}x'} = GS(t') = \begin{cases} G & (t' > 0), \\ 0 & (t' \leqslant 0) \end{cases} \tag{40}$$

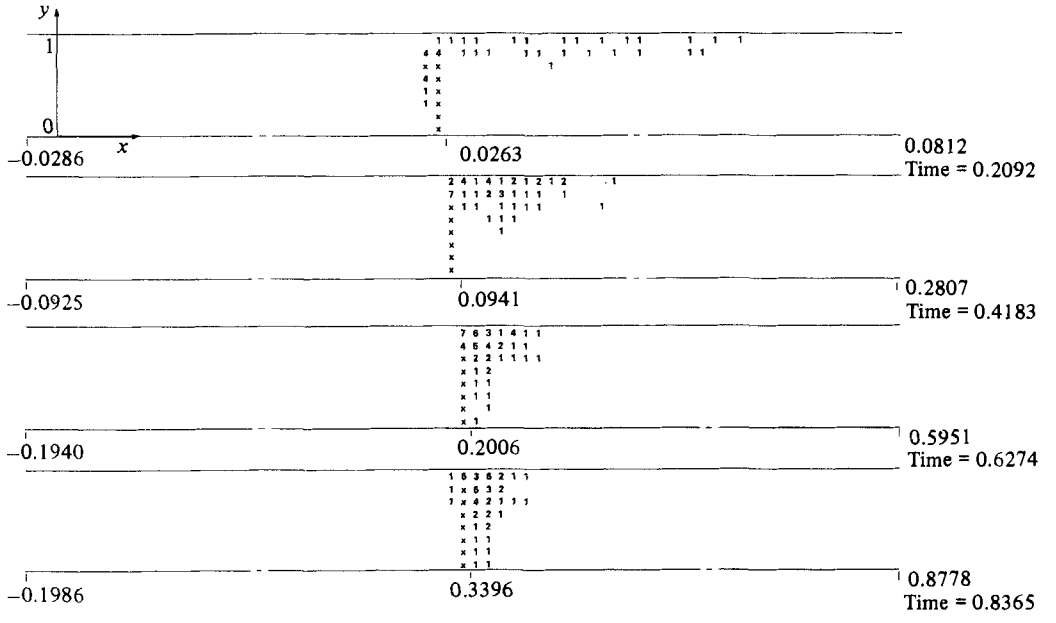

(a)

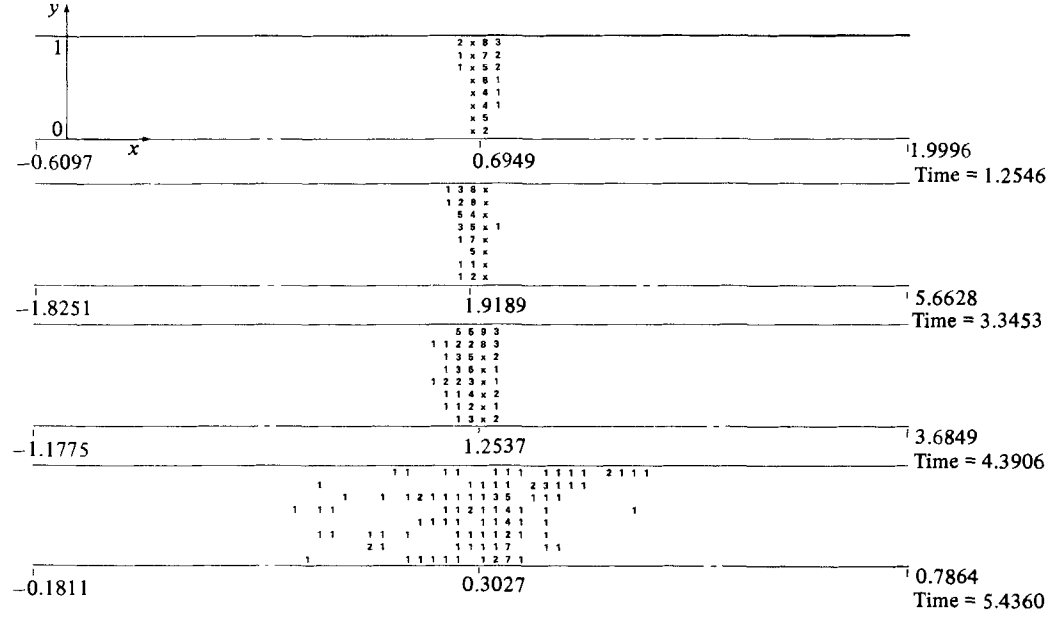

(b)

FIGURE 7. A numerical simulation of the evolution of a pulse of contaminant between parallel plates with an oscillating flow for which $\lambda = 20$ and $\gamma = 2\sqrt{2}$. The information is presented as in figure 5, and here a cross represents an offscale value.

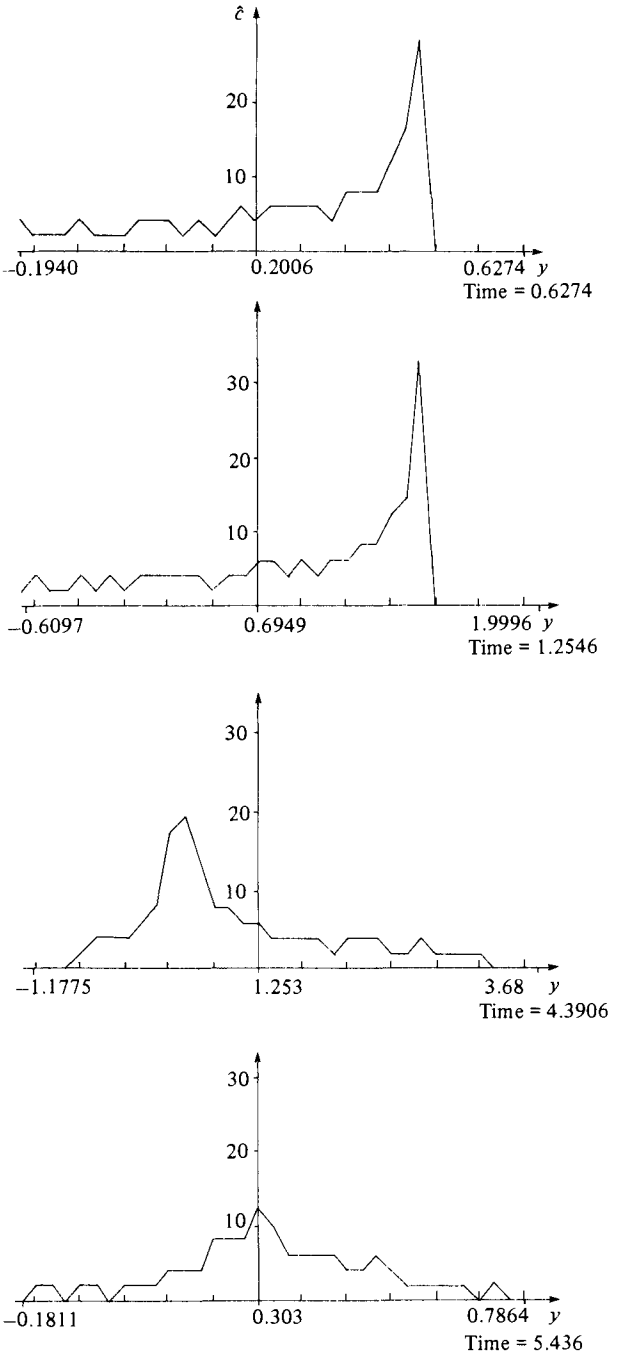

FIGURE 8. A summation over the depth of the values shown on figure 7 expressed as a percentage.

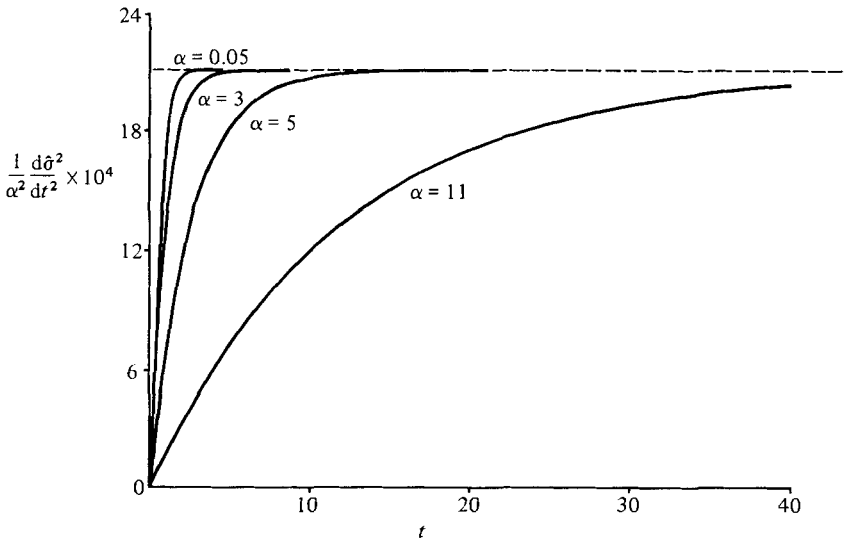

FIGURE 9. The evolution of dispersivity in impulsively started flow at various values of Schmidt number as given by (42).

is
$$u = \frac{1-y^2}{2} - \frac{2^4}{\pi^3} \sum_{\substack{n=1 \\ (\text{odd})}}^{\infty} \frac{e^{-(\frac{1}{2}n\pi)^2 t}}{n^3} \sin\left(\tfrac{1}{2}n\pi\,(y+1)\right), \tag{41}$$

where the variables are non-dimensionalized as $y = y'/a, t = t'\nu/a^2$, $x = (\nu^2/Ga^4)\,x'$ and $u = (\nu/a^2G)\,u'$. The summation in (41) represents the departure from the steady parabolic velocity profile of plane Poiseuille flow and reduces to zero at $t \gg 1$. For $t \ll 1$ the central ($y \sim 0$) part of u is relatively flat as the momentum boundary-layer grows across the conduit from $y = 1$. The longitudinal dispersivity can be constructed from (41), (22) and (13), and is

$$\begin{aligned}\frac{1}{2}\frac{d\hat{\sigma}(t)^2}{dt} = {} & \frac{2\alpha^2}{\pi^6} \sum_{m=1}^{\infty} \frac{1-e^{-(m\pi/\alpha)^2 t}}{m^6} \\ & + \frac{2^6\alpha^2}{\pi^8} \sum_{m=1}^{\infty} \sum_{\substack{n=1 \\ (\text{odd})}}^{\infty} \frac{(1-e^{-(m\pi/\alpha)^2 t})\,e^{-(\frac{1}{2}n\pi)^2 t}}{(n^2-4m^2)n^2m^4} - \frac{e^{-(\frac{1}{2}n\pi)^2 t} - e^{-(m\pi/\alpha)^2 t}}{(m^2-n^2\alpha^2)\,(p^2-4m^2)\,m^2p^2} \\ & + \frac{2^{11}}{\pi^8} \sum_{\substack{n,p=1 \\ (\text{odd})}}^{\infty} \sum_{m=1}^{\infty} \frac{e^{-((m\pi/\alpha)^2+(\frac{1}{2}n\pi)^2)t} \int_0^t e^{-((\frac{1}{2}p\pi)^2-(m\pi/\alpha)^2)\tau}\,d\tau}{(p^2-4m^2)\,(n^2-4m^2)\,n^2p^2},\end{aligned} \tag{42}$$

where $\alpha^2 = \nu/\kappa$ is the Schmidt number (see figure 9). The first term on the right-hand side of (42) is the longitudinal dispersivity for plane Poiseuille flow given in Dewey & Sullivan (1979), and the remaining terms provide the contribution made by the adjustment of the velocity profile to its asymptotic parabolic shape. The effect of these remaining terms in (42) can be seen always to reduce the dispersivity that would be achieved in plane Poiseuille flow. That is, if the velocity is decomposed into a steady (plane Poiseuille) u_S and transient u_T component as

$$u = u_S + u_T \tag{43}$$

then the longitudinal dispersivity from (13) is

$$\frac{1}{2}\frac{\mathrm{d}\hat{\sigma}^2}{\mathrm{d}t} = \frac{1}{2}\int_0^t\int_{-1}^1\int_{-1}^1 u_S(y)\,u_S(y_0)\,p(y,t-\tau;y_0)\,\mathrm{d}y_0\,\mathrm{d}y\,\mathrm{d}\tau - U(t)\int_{t_0}^t U(\tau)\,\mathrm{d}\tau$$
$$+\frac{1}{2}\int_0^t\int_{-1}^1\int_{-1}^1 u(y,t)\,u_T(y_0,\tau)\,p(y,t-\tau;y_0)\,\mathrm{d}y_0\,\mathrm{d}y\,\mathrm{d}\tau$$
$$+\int_0^t\int_{-1}^1\int_{-1}^1 u_S(y)\,u_T(y_0,t)\,p(y,t-\tau;y_0)\,\mathrm{d}y_0\,\mathrm{d}y\,\mathrm{d}\tau \qquad (44)$$

(where in (44) p and $U(t)$ are suitably non-dimensionalized) and since $u > 0$ and $u_T < 0$ for $t > 0$ and $-1 < y < 1$ the last two terms in (44) are negative. Hence the contribution of the impulsive start to plane Poiseuille flow is to reduce the longitudinal dispersivity. This is certainly evident on physical grounds (see (13)), since at no time in the development of $u(y,t)$ is there as much departure from $U(t)$ as when the flow is fully developed.

The ratio $R(t,\alpha)$ between the longitudinal dispersivity of an impulsively started flow to that in plane Poiseuille flow (i.e. the right-hand side of (42) divided by the first term on the right-hand side of (42)) is always less than or equal to unity. At $t \sim 0$, both from the observation from (41) that $u \sim t$ and also from an expansion of the exponential terms in (42), one observes that

$$R(t,\alpha) \sim t^2 \qquad (45)$$

and the ratio is independent of α. When $t \gg 1$ and $t/\alpha^2 \gg 1$

$$R(t,\alpha) \sim 1 \qquad (46)$$

as expected, and

$$\frac{1}{2}\frac{\mathrm{d}\hat{\sigma}^2}{\mathrm{d}t} = \frac{2\alpha^2}{945}. \qquad (47)$$

In order to achieve the constant value given in (47) it is necessary that $t/\alpha^2 \gg 1$, which, since α^2 is $O(10^3)$ in liquids, could be a very significant period of time and hence result in a very considerable contribution to dispersion from the impulsive start given to plane Poiseuille flow. Also, if $\alpha \sim 0$ and $t = O(1)$,

$$R(t,\alpha) \sim 1 - \frac{2^6}{945\pi^2}\sum_{m=1}^{\infty}\sum_{p=1}^{\infty}\frac{\mathrm{e}^{-(\frac{1}{2}n\pi)^2 t}}{m^4n^2(n^2-4m^2)}. \qquad (48)$$

Figure 10 shows the behaviour of $R(t,\alpha)$ that is calculated from (42) and illustrates the consequences of (45), (46) and (48).

The equivalent result to (42) can be established for the tube geometry. When u, the solution to

$$\frac{\partial u'}{\partial t'} = GS(t') + \frac{\nu}{r'}\frac{\partial}{\partial r'}\left(r'\frac{\partial u'}{\partial r'}\right), \qquad (49)$$

$$0 \leqslant r' \leqslant a, \quad u'(a,t') = 0, \qquad (50)$$

which in the non-dimensional variables $u = (\nu/a^2G)\,u'$, $x = \nu^2x'/Ga^4$, $r = r'/a$, $t = t'\nu/a^2$ is

$$u = 2\sum_{n=1}^{\infty}\frac{1-\mathrm{e}^{-\xi_n^2 t}}{\xi_n}\frac{J_0(r\,\xi_n)}{J_1(\xi_n)}, \qquad (51)$$

is used with (35) in the basic expression (13), the longitudinal dispersivity in an impulsively started flow in a tube becomes

$$\frac{1}{2}\frac{\mathrm{d}\hat{\sigma}^2(t)}{\mathrm{d}t} = 4\sum_{n,p,m=1}^{\infty}\frac{1-\mathrm{e}^{-\xi_m^2 t}}{(\xi_n^2-\eta_p^2)(\xi_n^2-\eta_p^2)}\int_0^t(1-\mathrm{e}^{-\xi_n^2\tau})\,\mathrm{e}^{-(\eta_p/\alpha^2)(t-\tau)}\,\mathrm{d}\tau. \qquad (52)$$

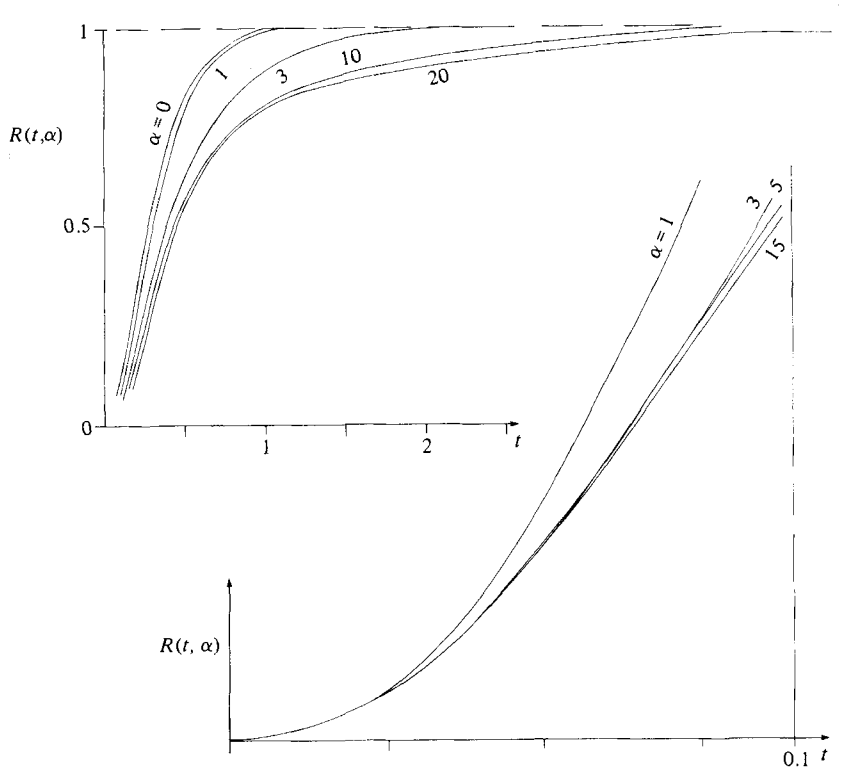

FIGURE 10. The evolution of the ratio of the variance growth rate in an impulsively started flow to that in plane Poiseuille flow $R(t, \alpha)$ for various values of the Schmidt number α.

The basic characteristics for the tube geometry are expected to be very similar to those of the parallel-plate geometry.

The authors wish to acknowledge the financial support of the Natural Sciences and Engineering Research Council of Canada.

Appendix A

Aris (1956) demonstrated a method whereby the moments of contaminant concentration distribution along an axial line within a conduit,

$$c^{(i)}(\boldsymbol{y}, t) = \int_{-\infty}^{\infty} x^i C(\boldsymbol{x}, t)\, \mathrm{d}x, \tag{A 1}$$

could be determined; and hence, in principle, with all of these moments the full contaminant concentration $C(x, t)$ could be compiled. In this specific comparison we take

$$\int C(\boldsymbol{x}, t)\, \mathrm{d}V(\boldsymbol{x}) = 1 \tag{A 2}$$

and define

$$M^{(i)}(t) = \int_V x^i C(\boldsymbol{x}, t)\, \mathrm{d}V(\boldsymbol{x}) = \int_A c^{(i)}(\boldsymbol{y}, t)\, \mathrm{d}A(\boldsymbol{y}). \tag{A 3}$$

Multiplication of each term in the convective-diffusion equation by x^i and integration over x results in

$$\frac{\partial c^{(i)}}{\partial t} = iuc^{(i-1)} + \kappa \nabla^2 c^{(i)} + i(i-1)\kappa c^{(i-2)} \tag{A 4}$$

with $$\frac{\partial c^{(i)}}{\partial n} = 0 \quad \text{on } \Gamma, \text{ the conduit boundary,} \tag{A 5}$$

and $$c^{(i)}(\boldsymbol{y}, 0) = c_0^{(i)}, \tag{A 6}$$

where ∇^2 is the two-dimensional Laplace operator and $c^{(i)} = 0$ for negative values of i. Integration of (A 4) over the conduit cross-section results in

$$\frac{\mathrm{d}}{\mathrm{d}t} M^{(i)} = i \int u(\boldsymbol{y}, t)\, c^{(i-1)}\, \mathrm{d}A(\boldsymbol{y}) + i(i-1)\,\kappa M^{(i-2)} \tag{A 7}$$

and $$M^{(i)}(0) = M_0^{(i)}. \tag{A 8}$$

With (A 4)–(A 8) all of the moments can be solved in terms of lower ordered moments. Here one is specifically interested in an initial distribution of $C(\boldsymbol{x}, t)$ that is a thin uniform sheet over the conduit cross-section and the variance growth rate, which in this notation is derived from

$$\frac{1}{2}\frac{\mathrm{d}\sigma^2}{\mathrm{d}t} = \frac{1}{2}\frac{\mathrm{d}}{\mathrm{d}t} M^{(2)} - M^{(1)} \frac{\mathrm{d}M^{(1)}}{\mathrm{d}t} = \int_A u(\boldsymbol{y}, t)\, c^{(1)}\, \mathrm{d}A(\boldsymbol{y}) + \kappa M^{(0)} - M^{(1)} \frac{\mathrm{d}M^{(1)}}{\mathrm{d}t}, \tag{A 9}$$

that is, using (A 7) with $i = 2$. One observes that with a uniform initial distribution within a uniform flow

$$c^{(0)}(\boldsymbol{y}, t) = \int_{-\infty}^{\infty} C(\boldsymbol{x}, t)\, \mathrm{d}x = \frac{1}{A}, \tag{A 10}$$

and hence $M^{(0)} = 1$; and using (A 7) with $i = 1$ one finds that

$$\begin{aligned} \frac{\mathrm{d}M^{(1)}}{\mathrm{d}t} &= \int_A u(\boldsymbol{y}, t)\, c^{(0)}\, \mathrm{d}A(\boldsymbol{y}) \\ &= U(t). \end{aligned} \tag{A 11}$$

Thus $$\frac{1}{2}\frac{\mathrm{d}\sigma^2}{\mathrm{d}t} = \int_A u(\boldsymbol{y}, t)\, c^{(1)}\, \mathrm{d}A(\boldsymbol{y}) + \kappa - U(t) \int_0^t U(\tau)\, \mathrm{d}\tau. \tag{A 12}$$

To complete the solution for the dispersivity given in (A 12), one requires the solution to (A 4)–(A 6) with $i = 1$; that is,

$$\frac{\partial c^{(1)}}{\partial t} = \frac{1}{A} u(\boldsymbol{y}, t) + \kappa \nabla^2 c^{(1)} \tag{A 13}$$

with $\partial c^{(1)}/\partial n = 0$ on the conduit boundary and $c^{(1)}(\boldsymbol{y}, 0) = 0$ corresponding to $C(\boldsymbol{x}, 0) = \delta(x)$.

Using the arguments of §2 one can write

$$c^{(1)}(\boldsymbol{y}, t) = \frac{1}{A} \int_0^t \int_A u(\boldsymbol{y}_0, t)\, p(\boldsymbol{y}, t-\tau; \boldsymbol{y}_0)\, \mathrm{d}A(\boldsymbol{y}_0)\, \mathrm{d}\tau, \tag{A 14}$$

where $p(\boldsymbol{y}, t; \boldsymbol{y}_0)$ is the probability density function obtained from the solution of (10)–(12). One now finds that (A 14) is actually the solution of (A 13), and thus the longitudinal dispersivity given by (A 12), and using (A 14) is

$$\frac{1}{2}\frac{\mathrm{d}\sigma^2}{\mathrm{d}t} = \frac{1}{A} \int_0^t \mathrm{d}\tau \int_A \mathrm{d}A(\boldsymbol{y}) \int_A \mathrm{d}A(\boldsymbol{y}_0)\, u(\boldsymbol{y}_0, t)\, u(\boldsymbol{y}, \tau)\, p(\boldsymbol{y}, t-\tau; \boldsymbol{y}_0) - U(t) \int_0^t U(\tau)\, \mathrm{d}\tau + \kappa. \tag{A 15}$$

The equation (A 15) is exactly (13) with the additive constant κ (which was left out in (13)) here included.

Appendix B

A numerical simulation of the diffusion of contaminant in the oscillating flow between parallel plates is provided by following the motion of typical contaminant molecules as these undergo a random walk on the Eulerian velocity field. The displacements at the end of one discrete time step $\Delta t'$ are

$$\Delta X' = \int_{t'}^{t'+\Delta t'} u'(Y'(\tau))\,\mathrm{d}\tau \pm L', \quad \Delta Y' = \pm L', \tag{B 1}$$

where $\pm L'$ is the randomly directed cross-stream constant step length. In principle this simple simulation is capable of providing an approximation to $C(\boldsymbol{x}, t)$ for arbitrary initial and boundary conditions; however, the computation time required may become prohibitive for complex flows and boundary conditions.

Some practical considerations in the implementation of the simulation to the oscillating flow between parallel plates follow. Non-dimensional variables as given in §3 are used. n contaminant molecules are initially spread out over $1-1/2n \geqslant y \geqslant 1/2n$ at uniform spacings of $1/n$ ($\frac{1}{2}$ the flow here because of the symmetry about $y = 0$). When the step size Δy is taken to be a multiple of $1/n$ each molecule will be constrained to occupy one of the n discrete locations on the cross-section, and hence the y-position of the molecule can be recorded as an integer value. The molecular diffusivity

$$\kappa = \tfrac{1}{2}w'L', \tag{B 2}$$

where $w' = \Delta y'/\Delta t'$ is the constant component of fluctuating molecular velocity in the y-direction, is unity in the non-dimensional variables in use, and

$$\Delta t = \tfrac{1}{2}\Delta y^2, \tag{B 3}$$

which, for $\Delta y = n^{-1}$, becomes

$$\Delta t = \frac{1}{2n^2}. \tag{B 4}$$

The molecules are reflected as they encounter $y = 1$ and $y = 0$, and because the molecules can only occupy n fixed positions the integral in (B 1) can be pretabulated (in part at least) as described in more detail in Jimenez (1982). Thus, structured in this way, a computer program needs as input information the value of λ (which determines the flow structure) and the number of molecules n to be used, and the result will be an approximation to $C(\boldsymbol{x}, t)$.

Errors occur because of a roundoff error in the addition of the calculated Δx of (B 1), because of the finite size of Δy, and because of imperfections in the random-number generator. Of these three sources of error the most problematic is that due to the finite size Δy. The value of Δy must be commensurately small with respect to the gradients of $u(\boldsymbol{y}, t)$. To accomplish this, and especially for the boundary-layer-type profiles when $\lambda \gg 1$, requires a significant increase in n, which gives a very large decrease in Δt as per (B 4) and leads to a tremendous increase in computation time to cover a complete cycle of the oscillating flow. The use of $n = 200$ results in a reasonably good representation with $\lambda = 2$ and $\gamma = 3\sqrt{2}$ where the errors in the mean and variance with respect to those calculated with (23) are less than 10 % when $5 < t < 23$. However, with $n = 400$ one expects no more than a reasonable qualitative result for the boundary-layer flow of $\lambda = 20$ and $\gamma = 2\sqrt{2}$ (the error in the mean at $t \sim 5$ is approximately 1 %, whereas the error in the variance is approximately 50 % there). The marginal costs in computing time necessary to improve the result by increasing n is extremely large.

REFERENCES

ALLEN, C. M. 1982 Numerical simulation of contaminant dispersion in estuary flows. *Proc. R. Soc. Lond.* A **381**, 179.

ARIS, R. 1956 On the dispersion of a solute in a fluid flowing through a tube. *Proc. R. Soc. Lond.* A **235**, 67.

CHATWIN, P. 1975 On the longitudinal dispersion of passive contaminant in oscillatory flows in tubes. *J. Fluid Mech.* **71**, 513.

CHATWIN, P. & SULLIVAN, P. 1984 The effect of the interaction between mean and fluctuating velocity components on turbulent dispersion in unsteady turbulent boundary layers. In *Proc. Vol. ASME Fluids Engng Conf., February 1984, New Orleans.*

DEWEY, R. & SULLIVAN, P. 1979 Longitudinal dispersion in flows that are homogeneous in the streamwise direction. *Z. angew. Math. Phys.* **30**, 601.

DEWEY, R. & SULLIVAN, P. 1982 Longitudinal-dispersion calculations in laminar flows by statistical analysis of molecular motions. *J. Fluid Mech.* **125**, 203.

JIMENEZ, C. 1982 On longitudinal dispersion in time-dependent flows. M.Sc. thesis, University of Western Ontario.

SCHLICHTING, H. 1960 *Boundary Layer Theory*, 4th edn. McGraw-Hill.

SMITH, R. 1982*a* Contaminant dispersion in oscillatory flows. *J. Fluid Mech.* **114**, 379.

SMITH, R. 1982*b* Non-uniform discharges of contaminants in shear flows. *J. Fluid Mech.* **120**, 71.

SMITH, R. 1983 The contraction of contaminant distributions in reversing flows. *J. Fluid Mech.* **129**, 137.

TAYLOR, G. I. 1921 Diffusion by continuous movements. *Proc. Lond. Math. Soc.* **20**, 196.

TAYLOR, G. I. 1953 dispersion of soluble matter in solvent flowing slowly through a tube. *Proc. R. Soc. Lond.* A **219**, 186.